frontiers in Materials

ORIGINAL RESEARCH
published: 20 April 2021
doi: 10.3389/fmats.2021.661999

4D Printing Pre-Strained Structures for Fast Thermal Actuation

*Yu Zou, Zhongyi Huang, Xiying Li and Pengyu Lv**

State Key Laboratory for Turbulence and Complex Systems, Department of Mechanics and Engineering Science, BIC-ESAT, College of Engineering, Peking University, Beijing, China

Four-dimensional (4D) printing is an emerging technology by adding the dimension of time-dependent reconfiguration into 3D printing. It enables the 3D printed structure to change the shape, property, or functionality under external stimuli such as temperature, magnetic field, and light, etc. Among the existing 4D printed structures, thermal responsive structures are widely used for their easy operation. However, the slow actuation of the thermal responsive structures impedes the applications like soft robotics. In the current work, a pre-strained strategy is proposed to accelerate the actuation of thermal responsive structures. A 4D printing platform that can apply strain during the printing process is constructed to fabricate the pre-strained structures under the aid of in-situ tensile of the printing base. A bilayer structure with one pre-strained layer and the other non-pre-strained layer is integrally printed. Through experiments and the finite element analysis, it is demonstrated that the aspect ratio has little effect on the deformation of the bilayer structure, whereas the pre-strain plays a key role in the deformation and also greatly accelerates the actuation of the bilayer structure. Based on the 4D printed pre-strained bilayer structure, an energy-free gripper is fabricated and a fully soft crawler is printed to achieve a high running speed.

Keywords: 4D printing, pre-strain, bilayer structure, thermal response, fast actuation

OPEN ACCESS

Edited by:
Yusheng Shi,
Huazhong University of Science and Technology, China

Reviewed by:
Feng Chen,
Zhejiang University of Technology, China
Xingzhe Wang,
Lanzhou University, China

***Correspondence:**
Pengyu Lv
lvpy@pku.edu.cn

Specialty section:
This article was submitted to Smart Materials, a section of the journal Frontiers in Materials

Received: *31 January 2021*
Accepted: *31 March 2021*
Published: *20 April 2021*

Citation:
Zou Y, Huang Z, Li X and Lv P (2021) 4D Printing Pre-Strained Structures for Fast Thermal Actuation. Front. Mater. 8:661999. doi: 10.3389/fmats.2021.661999

INTRODUCTION

3D printing is a widely used additive manufacturing technology that can embody objects from digital 3D models rapidly and inexpensively in contrast to traditional manufacturing techniques. By combining with smart materials, 3D printing is further extended to 4D printing with the addition of time-dependent response to external stimuli. 4D printing enables the printed structure to change its shape, property, and functionality under the external stimuli such as temperature (Ambulo et al., 2017; Ding et al., 2017; Kotikian et al., 2018), magnetic field (Kim et al., 2018, 2019; Zhu et al., 2018), light (Kuksenok and Balazs, 2016; Leist and Zhou, 2016; Yang et al., 2017), and pH (Nadgorny et al., 2016), etc. In view of the characteristics of shape morphing, applications of the 4D printed structure can be extended to diverse areas such as soft robotics (Kim et al., 2018, 2019; Kotikian et al., 2018; Yang et al., 2018; Zhu et al., 2018), origami (Ge et al., 2014; Liu et al., 2018; Teoh et al., 2018), biomedical device (Morrison et al., 2015; Gao et al., 2016; Zarek et al., 2017; Lin et al., 2020), tissue engineering (Villar et al., 2013; Li et al., 2016; Gill et al., 2018), and metamaterials (Xin et al., 2020), etc.

In consideration of the simplicity of operation and the applicability, the thermal responsive structure is one of the most widely used 4D printed structures. For example, the thermal responsive

hydrogel is used to realize programmable deformation of the soft sheet by patterning chemically distinct, fiber-like regions that exhibit different shrinkage and modulus under the external stimulus (Wu et al., 2013). Similarly, Naficy et al. (2017) print composite hydrogel structures which is capable of reversible deformation under the stimulus of hydration and temperature. Ge et al. (2013) fabricate thermal responsive 4D printed structure by printing shape memory polymer fibers in an elastomeric matrix. Although widely used in 4D printing, thermal responsive structures (Le Duigou et al., 2019; Nishiguchi et al., 2020) have a major problem in slow actuation resulting from the low heat conduction rate of the structures, especially the cooling rate.

In order to enhance the actuation rate of the thermal responsive structure, methods have been proposed. For example, Bartlett et al. (2017) increase the thermal conductivity by incorporating liquid metal microdroplets into the elastomer. Ze et al. (2020) report a novel magnetic shape memory polymer composite (M-SMP) that is softened by heating and actuated by a magnetic field. Based on this M-SMP, the structures can achieve faster actuation than conventional SMP-base structures (Ze et al., 2020). In spite of the current strategies for fast actuation of thermal responsive structure, there is still a long way to develop a simple and effective method to increase actuation speed of the thermal responsive structure.

Because the transmission rate of force is faster than the thermal conduction rate, it is an effective method to increase the actuation speed of the structure by combining mechanical response and thermal response. In this work, we construct a pre-strained 4D printing platform and propose a pre-strained strategy for fast actuation of 4D printed bilayer structures. Through experiments and finite element analysis (FEA), it is demonstrated that the aspect ratio has little effect on the deformation of the bilayer structure, whereas the pre-strain greatly affects the deformation and greatly increase the actuation speed of the thermal responsive structure. Based on this simple and effective strategy, we have designed a soft energy-free gripper with high responsive capacity and a soft crawler with a larger locomotion step and high speed. The current work provides a new solution based on pre-strain to increase the thermal actuation speed of 4D printed structures, which has a wide range of applications such as soft robotics with high locomotion speed, grippers with high responsive capacity and so on.

EXPERIMENTAL SETUP

Materials and Fabrication

A bilayer structure with one pre-strained layer (i.e., the thermal responsive layer) and the other non-pre-strained layer is integrally printed. For the fabrication of the thermal responsive layer, the precursors of Ecoflex^{TM} 00-35, Part A and Part B (Smooth-On, Inc.) were first mixed with ethanol (98%) in a volume ratio of 4:1, respectively. The well-mixed precursors of Ecoflex^{TM} 00-35, Part A and Part B were blended in a volume ratio of 1:1 for 4 min. Then, the mixture was poured into a mold and cured at room temperature for 5 min to obtain the ethanol-silicon composite. For the fabrication of the non-pre-strained layer, the base and curing agent of PDMS (polydimethylsiloxane, Dow Corning 184) were mingled in a mass ratio of 10:1. Then, the mixture was poured into a syringe and degassed for printing.

4D Printing Platform With Pre-Strain Stage

As shown in **Figure 1A**, the pre-strained 4D printing platform includes a 3D movement platform for spatial printing, and a clamping device fixed on a precision displacement table (**Figure 1B**) for applying the pre-strain. To show the printing capability of this pre-strained 4D printing platform, a bilayer structure consisting of a pre-strained bottom layer and a non-pre-strained top layer was printed. On the one hand, the bottom layer was made from the ethanol-silicon composite that is relatively soft (Young's modulus is 52 kPa) and can perform isotropic deformation under the thermal stimulation (Li et al., 2020). On the other hand, the top layer was fabricated with PDMS that is relatively stiff (Young's modulus is 2 MPa) and exhibits almost no expansion compared with the bottom layer fabricated of ethanol-silicon composite under the thermal stimulation (Schneider et al., 2009; Müller et al., 2019). Between the layers, resistance wire was embedded to provide the thermal stimulation. During printing as shown in **Figure 1C**, the bottom layer was stretched by the clamping device and served as the substrate for the printing of the top PDMS layer. Then, the resistance wire with a diameter of 0.15 mm was fixed by surface adhesion on the pre-stretched substrate and patterned into a zigzag line in order to increase the heating efficiency and reduce the impact on the deformation of the bilayer structure. Finally, the well-mixed PDMS precursor was squeezed out of the nozzle and heated at the nozzle by the resistance wire closely twisting around the nozzle (Hardin et al., 2015; Ober et al., 2015). 3 W was applied to the resistance wire of the nozzle to heat the PDMS precursor. After printing, the heated PDMS was cured at room temperature for 4 h.

Actuation Method

The printed bilayer structure is actuated by heating and cooling of the resistance wire embedded in the bilayer structure through a DC power. The DC power supply is connected to the resistance wire through the copper wires. The heating speed is regulated by the power. Increasing the current power will enhance the heating speed. The power is directly set to and remains 7 W for all the following experiments. The heated bilayer structure is cooled due to the natural heat dissipation after cutting off the power supply. The cooling rate depends on the thermal conductivity of the printed materials and the temperature difference, which is constant in our experiments.

DEFORMATION OF THE PRE-STRAINED BILAYERS

After 3D printing and releasing the pre-stretched substrate, the bilayer structure bends towards to bottom pre-stained layer. We denote the initial curvature as positive and the inverse bending curvature as negative. When the thermal stimulus is applied, the bottom layer begins to expand. As the temperature increase, the

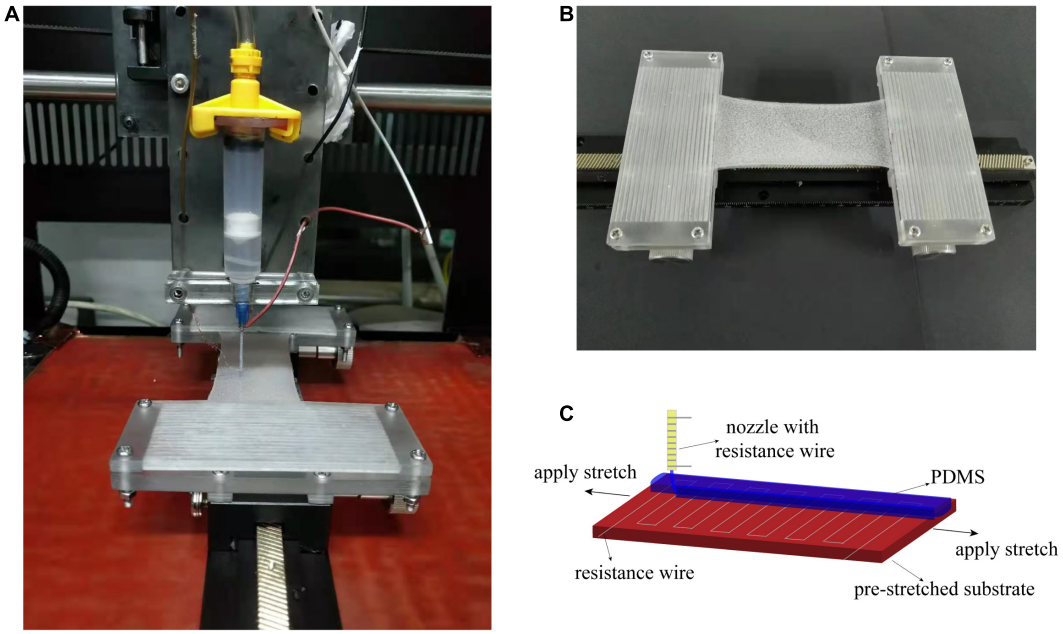

FIGURE 1 | Pre-strained 4D printing platform. **(A)** 3D movement platform for spatial printing. **(B)** The clamping device. **(C)** Schematic of the 4D printing with a pre-strain stage.

expansion of the bottom layer reaches the maximum swelling rate at the boiling point of ethanol, i.e., 78℃ and finally reaches the maximum deformation at 95℃ (Li et al., 2020). As shown in **Figure 2**, the slender and wide bilayer structure both bend towards to bottom layer for the pre-strain at the beginning. With the thermal stimulus applied, the bottom pre-strained layer made from the ethanol-silicon composite begins to expand while the top layer made from PDMS exhibits almost no expansion. For the expansion of the bottom layer, the mismatch strain between two layers as well as the curvature gradually decreases to zero. With further expansion of the bottom layer, the opposite mismatch strain between two layers appears, the bilayer structure bends upwards and the curvature becomes negative. Besides, the slender pre-strained bilayer structure whose width is much smaller than its length can be regarded as a beam and thus we can neglect the deformation in the width direction. For the wide pre-strained bilayer structure whose deformation in the width direction cannot be neglected, as the temperature increases, the curvature in the short-axis direction decreases, and the curvature in the long-axis direction increases. This phenomenon attributes to the isotropic expansion of the ethanol-silicon composite during the thermal stimulation. Combined with the powerful manufacturing capabilities of 3D printing, more pre-stretched structures have been fabricated (see details in **Supplementary Figure 1**).

To explore the deformation of a slender pre-strained bilayer structure, the effect of aspect ratio (length/width) and pre-strain on the deformation is experimentally investigated. **Figure 3** show the variation in the average curvature of the slender pre-strained bilayer structure as a function of the heating power of resistance wire. All the data in **Figure 3** represent the deformation of pre-strained bilayer structures with the width of 1 cm, and the thicknesses of the top and the bottom layers of 2 mm and 3 mm, respectively. **Figure 3A** shows the effect of the aspect ratio by changing the length of the bilayer structure from 3 cm to 4 cm and 5 cm under a constant pre-strain of 60%. **Figure 3B** shows the effect of the pre-strain by changing the pre-strain of the bottom layer from 40% to 60% and 80% under a constant structure length of 3 cm. The experimental data in **Figure 3** reflect that the average curvature decreases monotonically and nonlinearly as the heating power increases. Besides, the aspect ratio has less effect on the average curvature, while the pre-strain has much influence on the deformation of slender pre-strained bilayer structure.

Given the pre-strain ε_0, the curvature of the pre-strained bilayer structure κ can be predicted by the classical bi-strip model with the mismatch strain given by Timoshenko S.P (Timoshenko, 1925),

$$\kappa_{\text{Initial}} = \frac{6\varepsilon_0(1+m)^2}{h(1+\varepsilon_0)\left[3(1+m)^2+(1+mn)\left(m^2+\frac{1}{mn}\right)\right]}, \quad (1)$$

where m and n are the thickness ratio and Young's modulus ratio between the non-pre-strained layer and the pre-strained layer, respectively (see details in **Supplementary Text**). The solid lines and filled dots in **Figure 4** show the initial average curvatures of the pre-strained bilayer structure as a function of the pre-strain obtained by theory and experiments. All the structures in **Figure 4** have the same size, i.e., the length of 3 cm, the width of 1 cm, the thickness of the top layer of 2 mm, and the thickness of the bottom layer

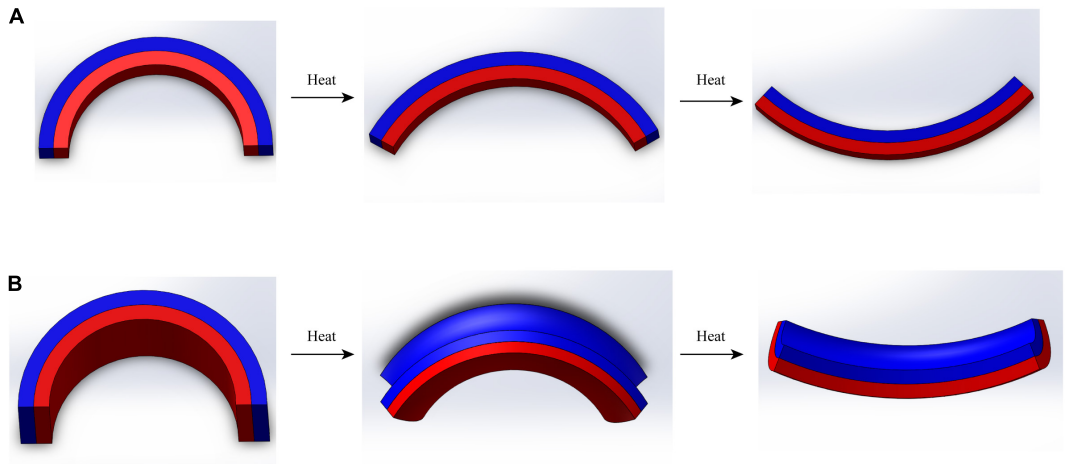

FIGURE 2 | Bi-directional deformation of pre-strained bilayer structure. Schematic of deformation of slender pre-strained bilayer structure **(A)** and of wide pre-strained bilayer structure **(B)**.

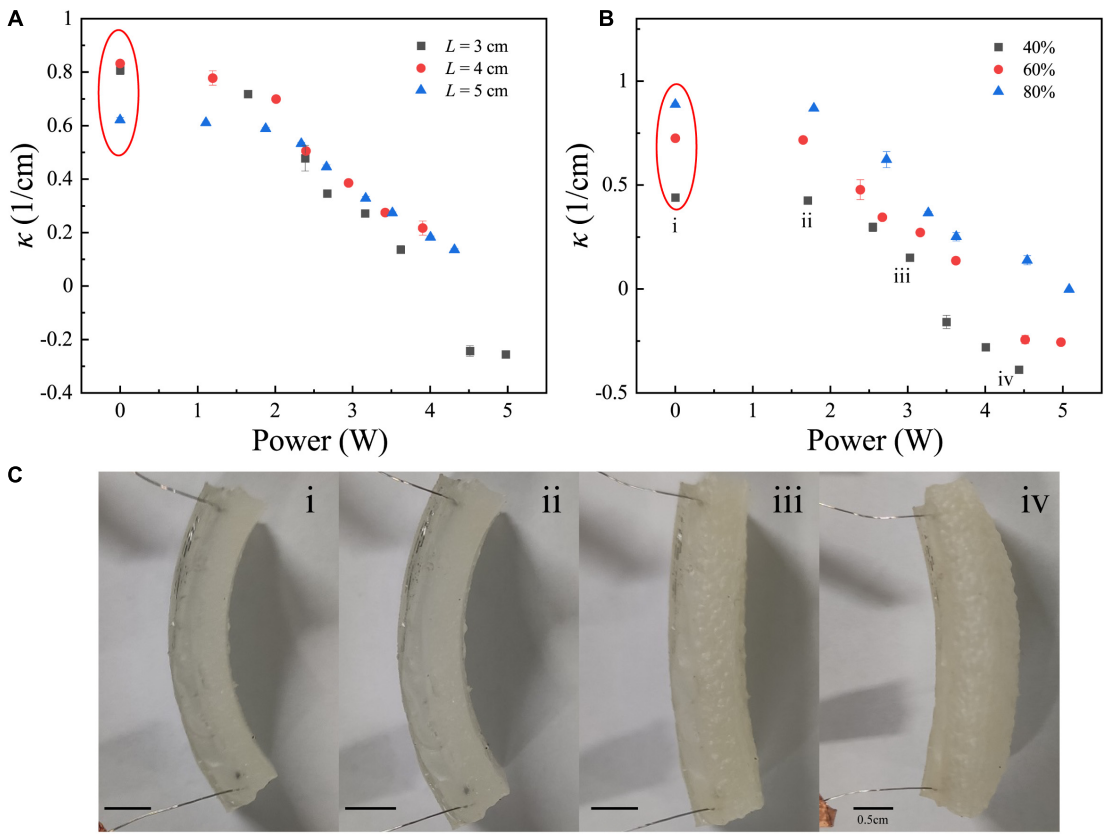

FIGURE 3 | Variation in the average curvature of the slender pre-strained bilayer structure. **(A)** Effect of the aspect ratio on the deformation under a constant pre-strain of 60%. **(B)** Effect of the pre-strain on the deformation under a constant structure length of 3 cm. **(C)** Deformation sequence as the thermal stimulus is applied to the bilayer structure with 40% pre-strain and 3-cm length.

of 3 mm. It is found that the data are in good agreement with the theoretical prediction when the pre-strain is smaller than 40%. When the pre-strain is greater than 40%, the experimentally measured values are slightly greater than the theoretical prediction. This deviation originates from the hypothesis of the theory that the constitutive relation of the model is linear elastic, whereas the materials in the experiments are hyperelastic.

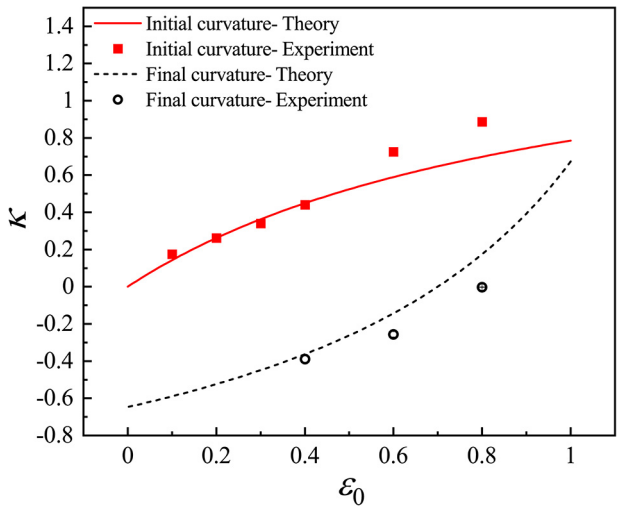

FIGURE 4 | The initial and final average curvatures of the slender pre-strained bilayer structure. Symbols are experimental data and lines are predictions of Equation (1) and (2). The solid lines and filled dots are the initial average curvatures and the dash lines and hollow dots are the final average curvatures.

The final curvatures of the pre-strained bilayer structures can be also predicted by the theory through introducing the maximum thermal expansion strain ε_{max} of the pre-strained layer. The final curvature is

$$\kappa_{Final} = \frac{6(\varepsilon_0 - \varepsilon_{max})(1 + m)^2}{h(1 + \varepsilon_0 - \varepsilon_{max})\left[3(1 + m)^2(1 + mn)\left(m^2 + \frac{1}{mn}\right)\right]}, \quad (2)$$

The maximum thermal expansion strain of our structures is nearly 70% obtained by experiment. Dash lines and hollow dots in **Figure 4** show the final curvatures as a function of the pre-strain, which presents a good agreement between the experimental data and the theoretical prediction.

For the wide pre-strained bilayer structure, Finite Element Analysis (FEA) is conducted by COMSOL Multiphysics to explore the effect of size and pre-strain on the deformation. The moduli of the top and the bottom layers in the FEA model are set to 2 MPa and 52 kPa, respectively. The coefficients of thermal expansion of the top and the bottom layers are 0 and 0.0025, respectively. As the temperature increases from 20℃ to 100℃, curvatures in two directions are analyzed for the wide pre-strained bilayer structure with the width of 2 cm as shown in **Figure 5**. For the cases of FEA simulation, three lengths of the bilayer structure (5 cm and 7 cm) are considered under a constant pre-strain of 20% and two pre-strains (10% and 20%) are considered under a constant length of 7 cm. As shown in **Figures 5A,B**, the curvature κ_1 decreases monotonically and the curvature κ_2 increases monotonically as the temperature increases. The curvature κ_1 and κ_2 increase notably as the pre-strain increases and are insensitive to the aspect ratio.

The effect of pre-strain on the deformation speed of wide curved bilayer structure is further explored. For the bilayer with pre-strain, it bends when it is released at the beginning without heating. While for the bilayer without pre-strain, we curve it as a control group. The relative length (L/L_0) of the curved bilayer is selected as the variable to measure the deformation as shown in **Figure 6A**. The sizes and materials of all the bilayer structures are the same, i.e., the length of 7 cm, the width of 2 cm, top layer (PDMS) thickness of 1 mm, bottom layer (ethanol-silicon composite) thickness of 2 mm. The heating power is 7 W. As shown in **Figure 6A**, as the temperature increases, the relative length of the structure increases and finally reaches to maximum deformation. And then, as the temperature decreases by stopping heating, the relative length decreases. According to the variation rate of L/L_0 during the heating and cooling process, it is demonstrated that the bilayer structure with 80% pre-strain has the fastest deformation speed both upon heating and cooling. Besides, the deformation amplitude of curved bilayer with 80% pre-strain is the largest. In comparison, the bilayer without pre-strain performs smaller deformation and takes longer time In **Figure 6B**, compared with other thermal responsive structures, the pre-strained bilayer structures present relatively fast deformation speed at centimeter scale (see **Supplementary Table 1**). Thus, the pre-strain can accelerate the actuation of the thermal responsive bilayer structure and provide a larger deformation amplitude.

APPLICATIONS OF PRE-STRAINED 4D PRINTING BILAYER STRUCTURE

In contrast to the slender bilayer structure, the wide bilayer structure has a larger contact area, which is more conducive forgrip and crawling. Thus, based on the wide bilayer structure (the length of 7 cm, the width of 2 cm, the PDMS layer thickness of 1 mm, and the ethanol-silicon composite layer thickness of 2 mm), a soft energy-free gripper with high responsive capacity and a soft crawler with a larger locomotion step and high speed are designed and presented in the following.

The wide pre-strained bilayer structure is first used to design a fast and energy-free gripper. In **Figure 7**, four identical wide pre-strained bilayers with 40% pre-strain act as fingers to form a soft gripper. In the absence of thermal stimuli, the wide pre-strained bilayer bends inwards and the soft gripper is in a close "finger" configuration. It is worth noting that the resistance wire is only embedded in the upper half section of the bilayer, namely the heating region as shown in **Figure 7A**. Such a design ensures the end of the "finger" maintain its initial shapes during the heating process so that this soft gripper can capture the object more efficiently. Furthermore, since the heating region is away from the end of the "fingers," the thermal stimuli has little effect on the object being held. By switching on and off the power supply, we can control the opening and closing of the gripper as shown in **Figure 7C**. Due to the pre-strain, our gripper can open or close the "fingers" quickly. It takes around 10 s to open the "fingers" as shown in **Figure 7A**. Furthermore, the energy-free gripper only needs energy to open the "fingers." After the gripper capturing the target object, the gripper can hold the object by its pre-strain without extra energy

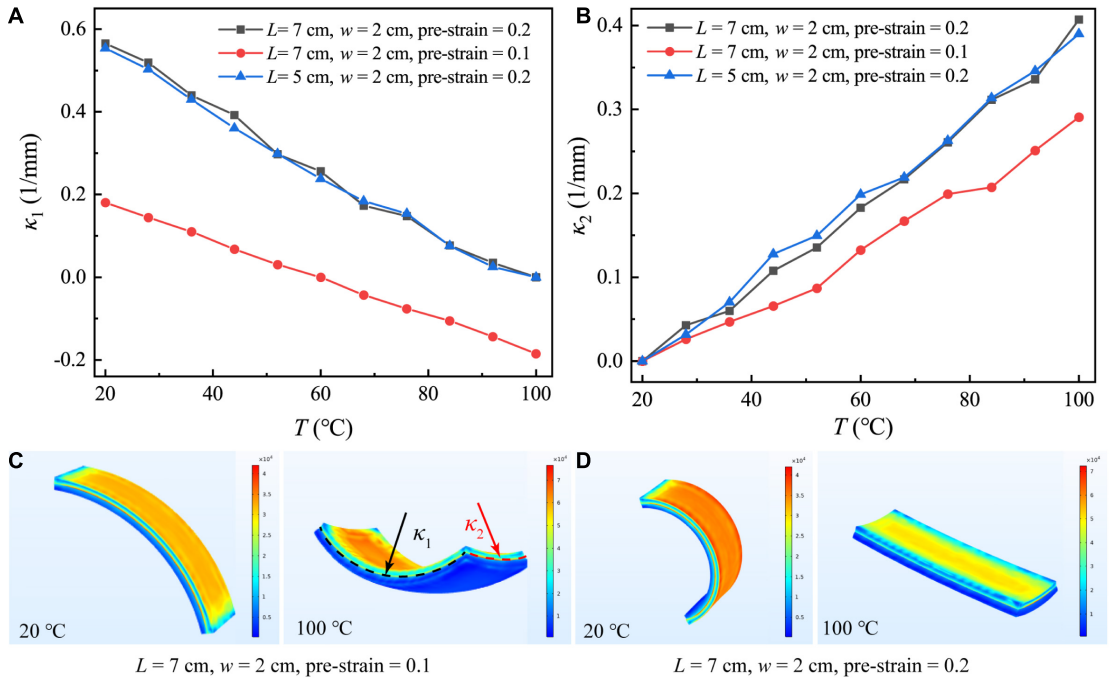

FIGURE 5 | FEA simulation results of wide pre-strain bilayer structure. **(A)** Variation in the curvature of pre-strained bilayer structure, **(A)** κ_1 and **(B)** κ_2, as a function of temperature for different aspect ratios and pre-strains. **(C,D)** The shapes of pre-strained bilayer structure with different aspect ratio at 20°C **(C)** and 100°C **(D)**.

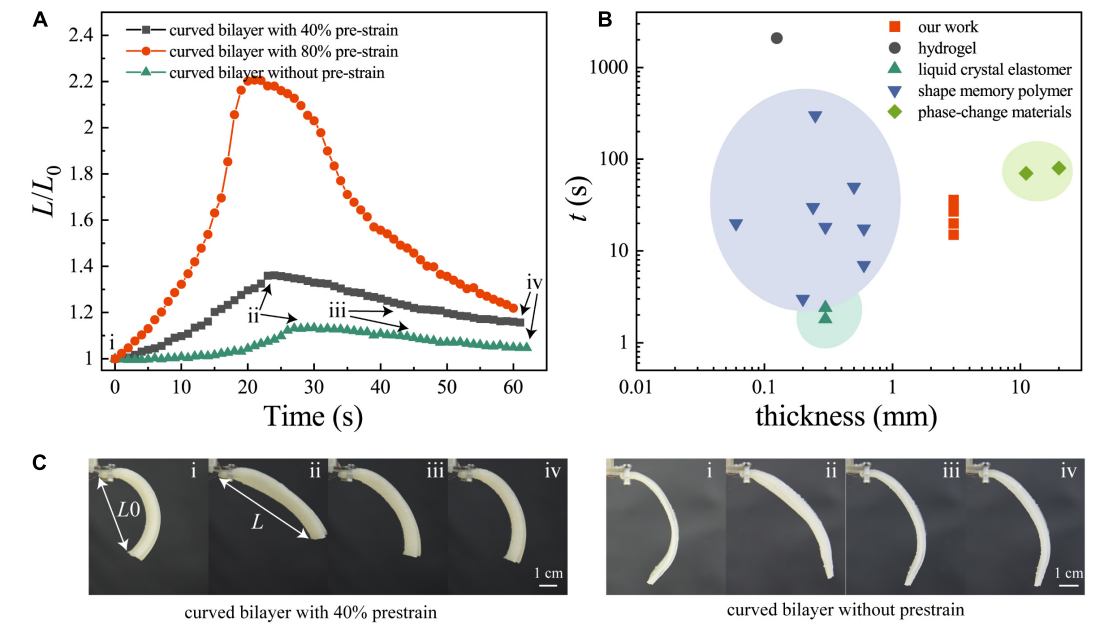

FIGURE 6 | Deformation of the wide bilayer. **(A)** The variation in the relative length of the curved bilayer as a function of time. **(B)** The comparison of deformation time between our work and other thermal responsive structures with different thicknesses in the literature. **(C)** Deformation sequence for bilayer with 40 % pre-strain (left) and without pre-strain (right).

input. **Figures 7D,E** shows that the gripper can grasp a sphere with a weight of 40 g, and a plastic cup filled with water with a weight of 70 g that is 3.5 times the whole weight of the soft gripper.

We further design and fabricate a soft crawler by utilizing the wide pre-strain bilayer structure. The resistance wire embedded in the structure is connected to the thin copper wire that supplies power for thermal actuation and avoids the effect on

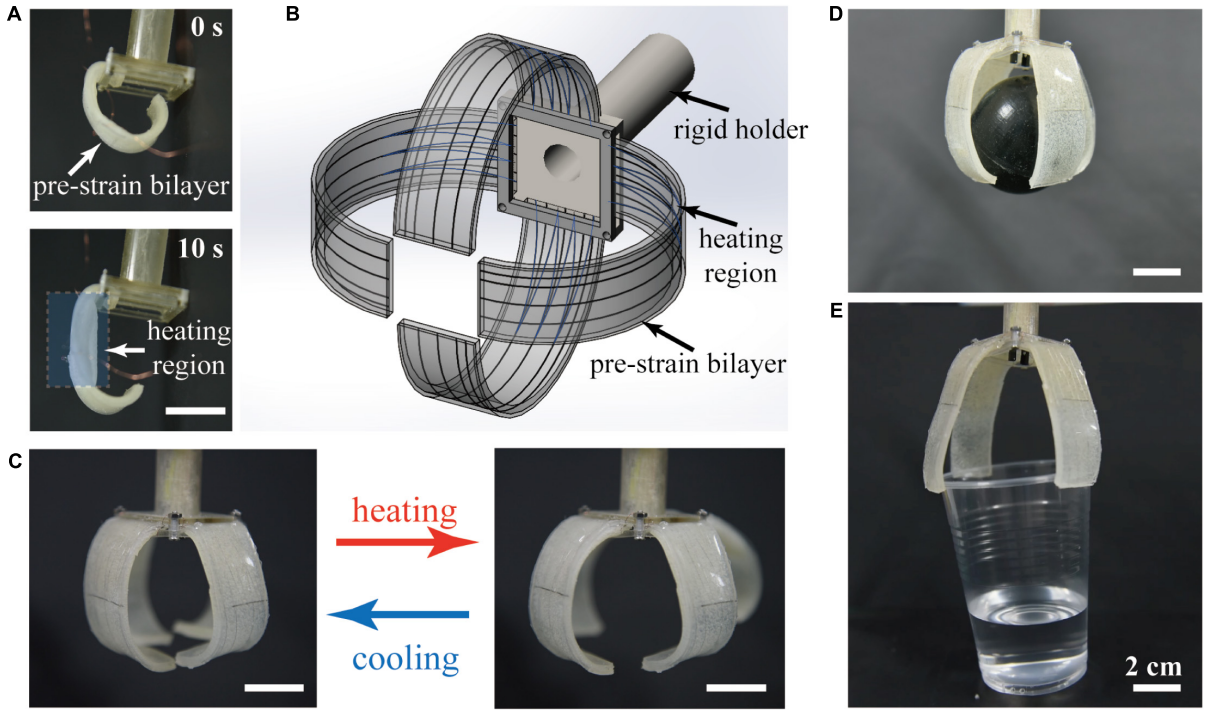

FIGURE 7 | Energy-free gripper based on 4D printing pre-strained bilayer. **(A)** Rapid deformation of pre-strained bilayer upon heating. **(B)** Schematic of pre-strained soft gripper composed of four identical pre-strained bilayers. **(C)** initial closed "fingers" open upon heating and closes upon cooling. **(D,E)** Demonstration of grasping of a sphere with a weight of 40 g, and a plastic cup filled with water with a weight of 70 g. The weight of the soft gripper is 20 g.

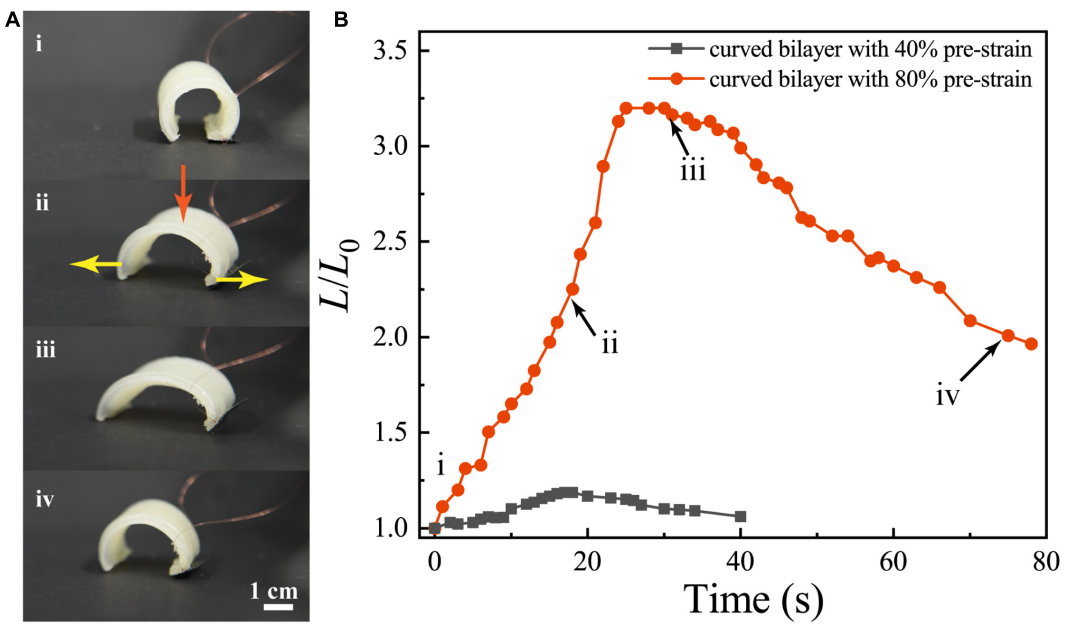

FIGURE 8 | Soft crawler based on 4D printing pre-strained bilayer. **(A)** Snapshot sequences for the crawler with 80 % pre-strain. **(B)** Deformation of the soft crawler as a function of time.

the locomotion of the crawler. To break the symmetry of the crawler and realize effective locomotion, two different flat sheets are attached to the end of the bilayer as shown in reference (Li et al., 2020). **Figure 8A** shows the locomotion mechanism of the soft crawler. During the heating-cooling cycle, the soft crawler can move forward effectively (**Supplementary Movie 1**)

Figure 8B shows the relative length of the soft crawler with different pre-strain over time. It is experimentally demonstrated that the soft crawler with a larger pre-strain (80%) has a larger motion step and higher speed, i.e., 0.3 mm/s, which is faster than the thermal actuation soft crawler of the previous work (Li et al., 2020).

CONCLUSION

In summary, a pre-strained strategy is proposed to accelerate the actuation of thermal responsive structures. To fabricate the pre-strained bilayer structure, we construct a pre-strained 4D printing platform that can apply strain to the substrate during the printing process. Due to the strain mismatch, the pre-strained layer tensions the non-pre-strained layer, leading to an initial bending of the printed structure. Because of the higher coefficient of thermal expansion of the inner pre-strained layer, the curvature of the pre-strained bilayer structure decrease under the external thermal stimulus. As the temperature increases, the initial bending structure will bend in the opposite direction. We have explored the effects of aspect ratio and pre-strain on the slender pre-strained bilayer structure through experiments and on the wide pre-strained bilayer structure through FEA. The deformation of pre-strained bilayer structure is less sensitive to the aspect ratio while sensitive to the pre-strain. Furthermore, we have studied the deformation speed of wide pre-strained bilayer structure with different pre-strains, and deduce that pre-strain can enhance the deformation speed of bilayer structure. Based on the pre-strained bilayer structure, we have designed a fast and energy-free gripper and a soft crawler with a larger motion step and higher speed. In further research, the pre-strained structure can be applied to more sophisticated soft robotics for higher responsive capacity.

DATA AVAILABILITY STATEMENT

The original contributions presented in the study are included in the article/**Supplementary Material**, further inquiries can be directed to the corresponding author.

AUTHOR CONTRIBUTIONS

PL and YZ conceived the idea and designed the research. YZ, ZH, and XL co-analyzed the experimental and calculated data. YZ, ZH, XL, and PL contributed to the writing and editing of the manuscript. All authors contributed to the article and approved the submitted version.

FUNDING

Financial support for this work was provided by the National Natural Science Foundation of China under Grant Nos. 91848201, 11988102, 11521202, 11872004, and 11802004.

SUPPLEMENTARY MATERIAL

The Supplementary Material for this article can be found online at: https://www.frontiersin.org/articles/10.3389/fmats.2021.661999/full#supplementary-material

REFERENCES

Ambulo, C. P., Burroughs, J. J., Boothby, J. M., Kim, H., Shankar, M. R., and Ware, T. H. (2017). Four-dimensional printing of liquid crystal elastomers. *ACS Applied Materials & Interfaces* 9, 37332–37339. doi: 10.1021/acsami.7b11851

Bartlett, M. D., Kazem, N., Powell-Palm, M. J., Huang, X., Sun, W., Malen, J. A., et al. (2017). High thermal conductivity in soft elastomers with elongated liquid metal inclusions. *Proceedings of the National Academy of Sciences of the United States of America* 114, 2143–2148. doi: 10.1073/pnas.1616377114

Ding, Z., Yuan, C., Peng, X., Wang, T., Qi, H. J., and Dunn, M. L. (2017). Direct 4D printing via active composite materials. *Science Advances* 3, e1602890. doi: 10.1126/sciadv.1602890

Gao, B., Yang, Q., Zhao, X., Jin, G., Ma, Y., and Xu, F. (2016). 4D bioprinting for biomedical applications. *Trends in Biotechnology* 34, 746–756. doi: 10.1016/j.tibtech.2016.03.004

Ge, Q., Dunn, C. K., Qi, H. J., and Dunn, M. L. (2014). Active origami by 4D printing. *Smart Materials and Structures* 23, 094007. doi: 10.1088/0964-1726/23/9/094007

Ge, Q., Qi, H. J., and Dunn, M. L. (2013). Active materials by four-dimension printing. *Applied Physics Letters* 103, 131901. doi: 10.1063/1.4819837

Gill, E. L., Li, X., Birch, M. A., and Huang, Y. Y. S. (2018). Multi-length scale bioprinting towards simulating microenvironmental cues. *Bio-design and Manufacturing* 1, 77–88. doi: 10.1007/s42242-018-0014-1

Hardin, J. O., Ober, T. J., Valentine, A. D., and Lewis, J. A. (2015). Microfluidic printheads for multimaterial 3D printing of viscoelastic inks. *Advanced Materials* 27, 3279–3284. doi: 10.1002/adma.201500222

Kim, Y., Parada, G. A., Liu, S., and Zhao, X. (2019). Ferromagnetic soft continuum robots. *Science Robotics* 4, doi: 10.1126/scirobotics.aax7329 **Q,

Kim, Y., Yuk, H., Zhao, R., Chester, S. A., and Zhao, X. (2018). Printing ferromagnetic domains for untethered fast-transforming soft materials. *Nature* 558, 274–279. doi: 10.1038/s41586-018-0185-0

Kotikian, A., Truby, R. L., Boley, J. W., White, T. J., and Lewis, J. A. (2018). 3D printing of liquid crystal elastomeric actuators with spatially programed nematic order. *Advanced Materials* 30, 1706164. doi: 10.1002/adma.201706164

Kuksenok, O., and Balazs, A. C. (2016). Stimuli-responsive behavior of composites integrating thermo-responsive gels with photo-responsive fibers. *Materials Horizons* 3, 53–62. doi: 10.1039/C5MH00212E

Le Duigou, A., Chabaud, G., Scarpa, F., and Castro, M. (2019). Bioinspired electro−thermo−hygro reversible shape−changing materials by 4D printing. *Advanced Functional Materials* 29, 1903280. doi: 10.1002/adfm.201903280

Leist, S. K., and Zhou, J. (2016). Current status of 4D printing technology and the potential of light-reactive smart materials as 4D printable materials. *Virtual and Physical Prototyping* 11, 249–262. doi: 10.1080/17452759.2016.1198630

Li, X., Duan, H., Lv, P., and Yi, X. (2020). Soft Actuators Based on Liquid-Vapor Phase Change Composites. *Soft Robotics* doi: 10.1089/soro.2020.0018 ***Q,

Li, Y. C., Zhang, Y. S., Akpek, A., Shin, S. R., and Khademhosseini, A. (2016). 4D bioprinting: the next-generation technology for biofabrication enabled by stimuli-responsive materials. *Biofabrication* 9, 012001. doi: 10.1088/1758-5090/9/1/012001

Lin, C., Zhang, L., Liu, Y., Liu, L., and Leng, J. (2020). 4D printing of personalized shape memory polymer vascular stents with negative Poisson's ratio structure: A preliminary study. *Science China Technological Sciences* 63, 578–588. doi: 10.1007/s11431-019-1468-2

Liu, G., Zhao, Y., Wu, G., and Lu, J. (2018). Origami and 4D printing of elastomer-derived ceramic structures. *Science Advances* 4, eaat0641. doi: 10.1126/sciadv.aat0641

Morrison, R. J., Hollister, S. J., Niedner, M. F., Mahani, M. G., Park, A. H., Mehta, D. K., et al. (2015). Mitigation of tracheobronchomalacia with 3D-printed personalized medical devices in pediatric patients. *Science Translational Medicine* 7, 285ra64. doi: 10.1126/scitranslmed.3010825

Müller, A., Wapler, M. C., and Wallrabe, U. (2019). A quick and accurate method to determine the Poisson's ratio and the coefficient of thermal expansion of PDMS. *Soft Matter* 15, 779–784. doi: 10.1039/C8SM02105H

Nadgorny, M., Xiao, Z., Chen, C., and Connal, L. A. (2016). Three-dimensional printing of pH-responsive and functional polymers on an affordable desktop printer. *ACS Applied Materials & Interfaces* 8, 28946–28954. doi: 10.1021/acsami.6b07388

Naficy, S., Gately, R., Gorkin, R. III, Xin, H., and Spinks, G. M. (2017). 4D printing of reversible shape morphing hydrogel structures. *Macromolecular Materials and Engineering* 302, 1600212. doi: 10.1002/mame.201600212

Nishiguchi, A., Zhang, H., Schweizerhof, S., Schulte, M. F., Mourran, A., and Möller, M. (2020). 4D printing of a light-driven soft actuator with programmed printing density. *ACS Applied Materials & Interfaces* 12, 12176–12185. doi: 10.1021/acsami.0c02781

Ober, T. J., Foresti, D., and Lewis, J. A. (2015). Active mixing of complex fluids at the microscale. *Proceedings of the National Academy of Sciences of the United States of America* 112, 12293–12298. doi: 10.1073/pnas.1509224112

Schneider, F., Draheim, J., Kamberger, R., and Wallrabe, U. (2009). Process and material properties of polydimethylsiloxane (PDMS) for Optical MEMS. *Sensors and Actuators A: Physical* 151, 95–99. doi: 10.1016/j.sna.2009.01.026

Teoh, J. E. M., An, J., Feng, X., Zhao, Y., Chua, C. K., and Liu, Y. (2018). Design and 4D printing of cross-folded origami structures: A preliminary investigation. *Materials* 11, 376. doi: 10.3390/ma11030376

Timoshenko, S. (1925). Analysis of bi-metal thermostats. *Josa* 11, 233–255.

Villar, G., Graham, A. D., and Bayley, H. (2013). A tissue-like printed material. *Science* 340, 48–52. doi: 10.1126/science.1229495

Wu, Z. L., Moshe, M., Greener, J., Therien-Aubin, H., Nie, Z., Sharon, E., et al. (2013). Three-dimensional shape transformations of hydrogel sheets induced by small-scale modulation of internal stresses. *Nature Communications* 4, 1–7. doi: 10.1038/ncomms2549

Xin, X., Liu, L., Liu, Y., and Leng, J. (2020). 4D Printing Auxetic Metamaterials with Tunable, Programmable, and Reconfigurable Mechanical Properties. *Advanced Functional Materials* 30, 2004226. doi: 10.1002/adfm.202004226

Yang, H., Leow, W. R., Wang, T., Wang, J., Yu, J., He, K., et al. (2017). 3D printed photoresponsive devices based on shape memory composites. *Advanced Materials* 29, 1701627. doi: 10.1002/adma.201701627

Yang, Y., Li, Y., and Chen, Y. (2018). Principles and methods for stiffness modulation in soft robot design and development. *Bio-Design and Manufacturing* 1, 14–25. doi: 10.1007/s42242-018-0001-6

Zarek, M., Mansour, N., Shapira, S., and Cohn, D. (2017). 4D printing of shape memory-based personalized endoluminal medical devices. *Macromolecular Rapid Communications* 38, 1600628. doi: 10.1002/marc.201600628

Ze, Q., Kuang, X., Wu, S., Wong, J., Montgomery, S. M., Zhang, R., et al. (2020). Magnetic shape memory polymers with integrated multifunctional shape manipulation. *Advanced Materials* 32, 1906657. doi: 10.1002/adma.201906657

Zhu, P., Yang, W., Wang, R., Gao, S., Li, B., and Li, Q. (2018). 4D printing of complex structures with a fast response time to magnetic stimulus. *ACS Applied Materials & Interfaces* 10, 36435–36442. doi: 10.1021/acsami.8b12853

Conflict of Interest: The authors declare that the research was conducted in the absence of any commercial or financial relationships that could be construed as a potential conflict of interest.